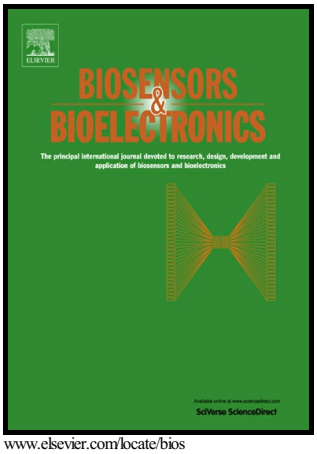

www.elsevier.com/locate/bios

Highly sensitive paper-based immunoassay using photothermal laser speckle imaging

Seungri Song, Seoyeon Choi, Suho Ryu, Soocheol Kim, Tongwha Kim, Joonchul Shin, Hyo-Il Jung, Chulmin Joo

PII: S0956-5663(18)30456-1
DOI: https://doi.org/10.1016/j.bios.2018.06.024
Reference: BIOS10544

To appear in: *Biosensors and Bioelectronic*

Received date: 28 April 2018
Revised date: 8 June 2018
Accepted date: 8 June 2018

Cite this article as: Seungri Song, Seoyeon Choi, Suho Ryu, Soocheol Kim, Tongwha Kim, Joonchul Shin, Hyo-Il Jung and Chulmin Joo, Highly sensitive paper-based immunoassay using photothermal laser speckle imaging, *Biosensors and Bioelectronic,* https://doi.org/10.1016/j.bios.2018.06.024

Highly sensitive paper-based immunoassay using photothermal laser speckle imaging

Seungri Song[a,1], Seoyeon Choi[b,1], Suho Ryu[a], Soocheol Kim[a], Tongwha Kim[c], Joonchul Shin[a], Hyo-Il Jung[a], and Chulmin Joo[a,*]

[a] Department of Mechanical Engineering, Yonsei University, 50 Yonsei-ro, Seodaemoon-gu, Seoul, 03722, Republic of Korea

[b] Mirimedix Inc., 43, Geodudanji 1-gil, Chuncheon, Gangwon-do, Republic of Korea

[c] Department of Mechanical & Industrial Engineering, University of Toronto, Ontario M5S 1A1, Canada

*Corresponding Author.

E-mail address : cjoo@yonsei.ac.kr (C. Joo)

[1] The authors contributed equally to this work

ABSTRACT

Paper-based lateral-flow assay (LFA) is a simple and inexpensive point-of-care device that has become commonplace in medicine, environmental monitoring, and over-the-counter personal use. Some LFAs have demonstrated comparable analytical performance with laboratory-based methods, but the detection limit or sensitivity of most LFAs is significantly inferior to other molecular techniques by 10–100x. Consequently, LFAs are not viable for the early detection of disease-relevant biomarkers that are present in extremely small amounts in clinical specimens. Herein, we present a simple, cost-effective, and highly sensitive LFA sensor based on photothermal laser speckle imaging (PT-LSI). Under the illumination of a photothermal excitation light, gold nanoparticles (AuNPs), a common signal transduction medium in LFAs, absorb the light energy to produce heat, which subsequently induces modulation of the optical property and thermal deformation of the membrane. We measured these fluctuations through laser speckle imaging to quantify the concentration of AuNP-biomarker complexes. We experimentally demonstrate that the detection limit of our technique is superior to that of colorimetric detector by 68–125x. The capability of our sensor for highly sensitive detection of disease biomarkers is validated by using U.S. FDA-approved LFA kits for cryptococcal antigens (CrAg).

KEYWORDS: Paper-based lateral flow immunoassay, Photothermal, Laser speckle imaging, Optical sensor

1. Introduction

Paper-based lateral flow immunoassay is a rapid and simple analytical method for screening biomarkers in complex biological fluids (Ngom et al. 2010; Posthuma-Trumpie et al. 2009). LFA requires minimal effort for specimen preparation and overall measurement procedure, and has thus been broadly employed for clinical diagnosis (Martinez et al. 2010; Ngom et al. 2010), healthcare monitoring (Martinez et al. 2010), and personal use (Leuvering et al. 1980). For instance, LFA chips for human immunodeficiency virus (HIV) and hepatitis C virus screening have been available to the general population for several years, and LFA for pregnancy tests can be readily bought over the counter. Paper-based LFAs have recently been explored for measuring infectious agents (Whang and Um 2005; Xia et al. 2009), food quality control (Kim et al. 2015; Tripathi et al. 2017), and environmental monitoring (Mauriz et al. 2007; Zhu et al. 2008).

LFA chips typically employ a nitrocellulose membrane as the base substrate of the detection chip, of which a specific region is functionalized with capturing antibodies. When carry out an assay, the chip is dipped in the clinical specimen, and the target analytes, if present in the specimen, bind to antibody-coated metallic nanoparticles, such as AuNPs, in the conjugation pad. This complex, consisting of antigen-antibody-AuNPs, then moves within the membrane through capillary action, and is stopped when a capturing antibody in the membrane recognizes the complex. This interaction and recognition process results in the accumulation of AuNPs in a specific region of the membrane, producing a change in visual contrast.

Colorimetric analysis is commonly used to measure these color changes and determine the presence of the analytes in the specimen. This method enables detection with the naked eye if

the number of accumulated AuNPs is large; however, the result is qualitative, and its sensitivity and detection limits are inferior to those of lab-based analyzers. Specifically, the detection limit of most LFA methods is in the millimolar to micromolar range (Liu et al. 2006; Posthuma-Trumpie et al. 2009), while the assay for disease-relevant biomolecules requires a detection limit in the sub-micromolar range. In order to improve LFA sensitivity, various detection strategies have been developed based on fluorescence, electrochemistry, and chemiluminescence. Fluorescence-based detectors (Ahn et al. 2003; Khreich et al. 2008) typically exhibit 10 to 1000 times higher sensitivity compared with the colorimetric sensor. However, the operation of fluorescence sensors involves complicated and time-consuming preparation procedures, and the measurements are susceptible to artifacts such as photo-bleaching and photochemical degradation. Electrochemistry- and chemiluminescence-based sensors have also been demonstrated as high-sensitivity LFA detectors (Lin et al. 2008; Maiolini et al. 2014; Mirasoli et al. 2012). Yet, these sensors require specific markers that exhibit electrical and optical responses upon the recognition of antigens. Electrochemistry sensors require the membranes to be patterned with electrodes, and complex fabrication procedures are therefore required for integrating all the components on a chip (Quesada-González and Merkoçi 2015).

High-sensitivity LFA detectors based on the plasmonic nature of AuNPs have recently been demonstrated. Metallic nanoparticles such as the AuNPs exhibit localized surface plasmon resonance (LSPR), which manifests as enhanced light absorption and a strong photothermal (PT) response at the plasmon resonance frequency. Hence, the particles, under the illumination of light of the resonance frequency, absorb the light energy and convert it into heat. Recently,

thermal imaging of LFA chips was performed in a high-sensitivity LFA sensor (Qin et al. 2012). This sensor demonstrated a sensitivity 32 times higher than that of colorimetric sensors, but an expensive infrared camera was utilized to map the spatial temperature distribution across the membrane. Zhao *et al.* also demonstrated a high-sensitivity photoacoustic LFA sensor (Zhao et al. 2016). With this type of sensor, the acoustic signals generated by the AuNPs under PT light illumination were measured to quantify the analyte concentrations. The sensor exhibited a sensitivity 3-33 times higher than colorimetric sensors, but the LFA chip and the acoustic sensors should be enclosed in a sound-insulation chamber, making the system bulky and expensive.

Here, we demonstrate a simple, inexpensive, and highly sensitive LFA detector based on photothermal laser speckle imaging. PT-LSI exploits high sensitivity of laser speckle imaging to the changes in the optical and structural features to detect the species of interest in diffuse materials. Upon the illumination of an LFA membrane with a probe light, the light undergoes multiple scattering inside it and produces a speckle pattern on an image sensor. The membrane is then illuminated by a PT excitation light with its wavelength matched to the LSPR absorption band of the AuNPs. The particles then absorb the PT light energy and generate heat, which subsequently leads to the modulation of the refractive index and thermal deformation of the membrane. This change is measured via laser speckle imaging. We present the PT-LSI operation, and experimentally demonstrate 125x improved detection limit of PT-LSI, compared with colorimetric detectors for AuNP-spotted membranes. The capability of our sensor for clinical LFA is then validated by measuring an U.S. FDA-approved CrAg LFA, indicating a 68x improved detection limit.

2. Materials and method

2.1. PT-LSI operation

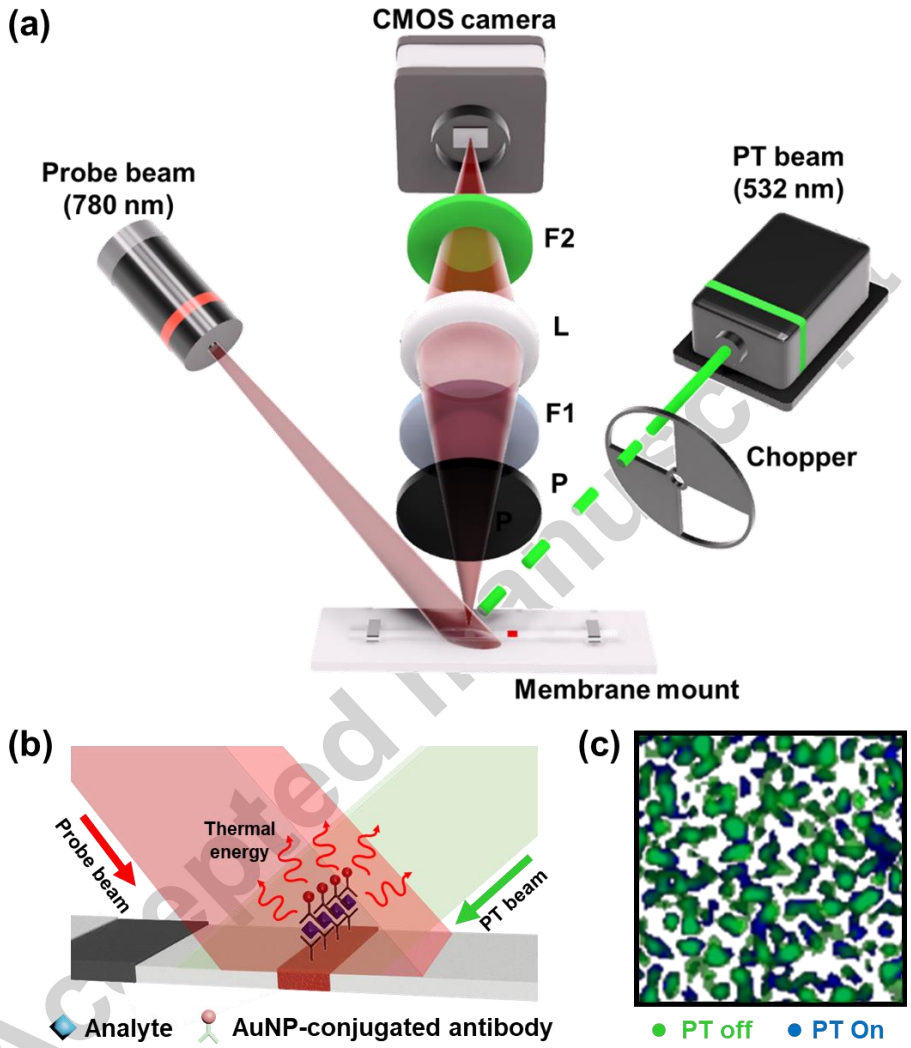

Fig. 1. Schematic of the PT-LSI sensor. (a) A 780-nm light illuminates an LFA membrane. The light is scattered through the membrane and the interference of the scattered light produces a speckle pattern on the image sensor. The sensing region is then illuminated by a 532-nm light, which is absorbed by the AuNPs. (b) The absorbed light energy is converted into heat, and the resultant temperature increase alters the speckle pattern. (c) Exemplary speckle images before (green) and after (blue) PT illumination. The measurement of the speckle pattern modulation enables the quantification of biomarkers in the specimen.

Fig. 1a depicts a schematic of our PT-LSI sensor. A linearly polarized 780-nm light from a laser pointer (AiXiZ, USA) obliquely illuminated an LFA membrane (after complete reaction) over an extended area. Due to the random fibrous structure of the membrane, the light undergoes multiple scattering, and the interference of the scattered light produces a speckle pattern on an image sensor (Lt225, Lumenera, Canada). Speckle patterns are extremely sensitive to perturbations of the refractive index and structural features of the media, and thus have been broadly utilized in diverse metrological and biomedical applications (Briers and Webster 1996; Huang et al. 2009; Hung et al. 2009; Stolyarov et al. 2015). In our PT-LSI operation, the LFA membrane is illuminated by additional 532-nm light (MGL-lll-532, continuous wave, CNI Laser, China), namely PT excitation light, whose wavelength is in the LSPR range of the AuNPs. The AuNPs in the sensing region then absorb the PT light energy and convert it into thermal energy (Fig. 1b). The resultant increase in temperature alters the refractive index in the vicinity of the AuNPs and causes thermal deformation of the membrane, which subsequently modulates the speckle pattern (Fig. 1c). Measuring this change allows for quantification of the biomarker-AuNP complexes. Measurements of speckle pattern modulation can be carried out either under continuous or intensity-modulated PT light illumination. In practice, though, external disturbances, such as vibration and laser intensity noise, may affect the measurements. Therefore, we employed an intensity-modulation scheme, which allowed for highly sensitive measurement of speckle pattern changes (Supplementary Information). The PT light Intensity modulation was implemented by placing an optical chopper system (MC2000B, Thorlabs, USA) in the PT beam path. The time-lapse speckle images were acquired at 30 Hz over a period of 20

seconds, and processed as described in Section 2.2. In our case, operating PT-LSI with 2-Hz PT light modulation provided the measurement with the highest signal-to-noise ratio (SNR) and smallest detection limit (Figs. S2 and S3). A detailed description of our PT-LSI setup is given in Supplementary Information.

2.2. PT-LSI signal processing

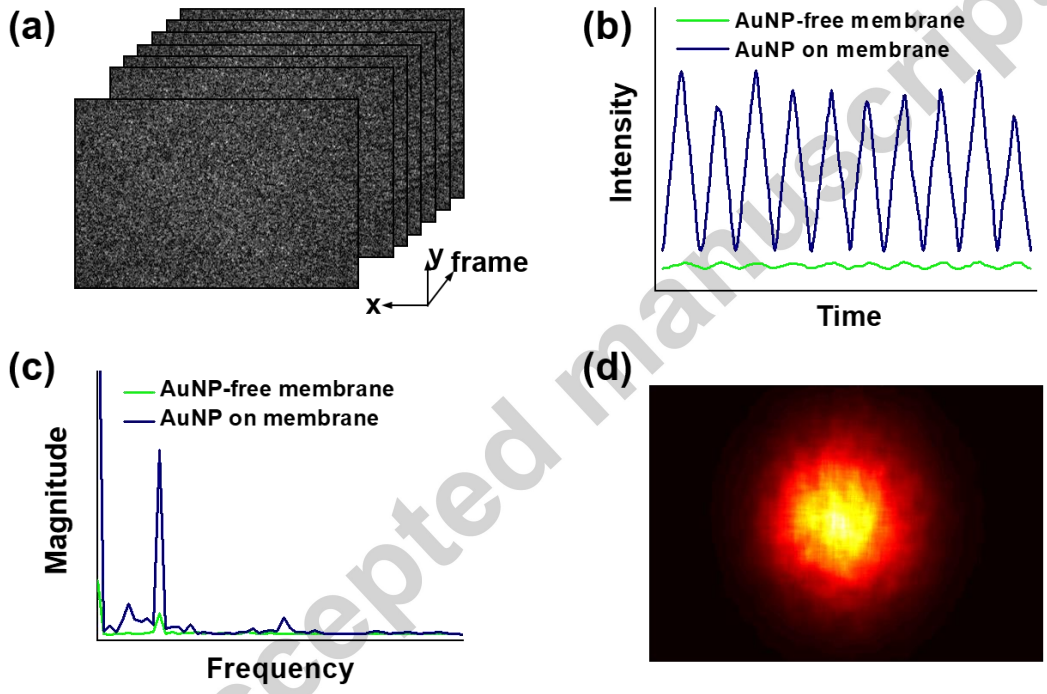

Fig. 2. PT-LSI signal processing procedure. (a) Representative speckle images during modulated PT light modulation. (b) Exemplary pixel intensity fluctuations in the speckle images. Note that the magnitude of the intensity fluctuation from the AuNP-spotted membrane is markedly larger than that from the AuNP-free membrane. (c) Magnitude of the Fourier transform of the intensity fluctuations shown in (b). The PT-LSI signal is the magnitude at the modulation frequency. (d) Representative PT-LSI image obtained by mapping the signals in two-dimensional space.

The signal processing procedure for the PT-LSI sensor output is outlined in Fig. 2. For time-lapse images of the speckle pattern during modulated PT light illumination (Fig. 2a), the intensity in each pixel is characterized by a fluctuation at the same frequency of the PT light modulation (Fig. 2b). Note that this intensity fluctuation is caused largely by PT response of AuNPs in the membrane. The pixel intensity in the AuNP-free regions also exhibited oscillation with a much smaller magnitude, which may be in part accounted for by the intrinsic PT response of the membrane. The measured intensity fluctuation in each pixel is then Fourier transformed, and its magnitude at the PT modulation frequency is measured (Fig. 2c). We perform this operation on each pixel, and the obtained magnitudes are mapped onto the corresponding pixels to generate a PT-LSI image (Fig. 2d). The average of the PT-LSI signals over a region of interest (ROI), termed "PT-LSI output", is calculated to quantify AuNP concentration and, thus, the concentration of the analytes of interest. The signal processing was conducted using a custom-built program implemented in MATLAB (R2017a, MathWorks, USA).

2.3. Colorimetric analysis

We performed colorimetric analysis of the LFA membranes to compare detection performance of PT-LSI vs. colorimetric sensor. For colorimetric assay, color images of the membranes were acquired using a custom-built colorimetric sensor (Supplementary Information). The acquired color images were split into the red (R), green (G), and blue (B) channels, and we computed the mean pixel values of the G channel from the ROI (G_{ROI}) and the AuNP-free region (G_0). The difference of the two quantities, or $G_0 - G_{ROI}$, was then computed

as the colorimetric output to compensate for the background noise arising from membrane and light source fluctuations. Details of the colorimetric sensor and analysis are provided in Supplementary Information.

2.4. AuNP-spotted nitrocellulose membranes

AuNP solutions of various concentrations were prepared by two-fold dilution of bare AuNP suspensions (753629, Sigma-Aldrich, USA) in 0.1 mM PBS to obtain solutions in the range of 1.14×10^{9} to 1.44×10^{12} NPs/mL. To prepare AuNP solutions of higher concentrations than the stock solution, the AuNPs were enriched by centrifugation at 4000 g for 30 min at 4 °C. The pellets were re-suspended in 0.1 mM PBS and stored at 4 °C until used. The size of the AuNPs was measured to be 30 nm, with a size distribution of CV < 10 %. 1 µL of each AuNP solution was pipetted onto nitrocellulose membranes (HF13502XSS, Millipore, USA) and dried in air for 10 min.

2.5. Cryptococcal antigen lateral flow assay

The FDA-approved CrAg LFA was purchased from IMMY Inc. (CR2003, Norman, USA). We prepared a series of CrAg-positive solutions of various concentrations by diluting the CrAg-positive solution provided in the CrAg LFA kit. After five-fold dilution of the positive control, two-fold serial dilutions were conducted, down to 1:81920 CrAg titer. The LFA paper strips were then submerged into 80 µL of each solution for 10 min at room temperature. The LFA strip was taken out and dried for 10 min.

3. Results

3.1. PT-LSI imaging of AuNP-spotted membranes

We first performed PT-LSI imaging of AuNP-spotted membranes to assess its viability for highly sensitive LFA detection. A phosphate buffer saline (PBS) and two AuNP solutions with concentrations of 1.12×10^{11} and 1.44×10^{12} NPs/mL were prepared, and 1 μL of each solution was pipetted onto the membrane. Colorimetric and PT-LSI measurements were then performed approximately 10 minutes after the membranes were dried. For PT excitation, a 532-nm laser modulated at 2 Hz was used to illuminate the membrane with the measured optical irradiance of 1.5 mW/mm^2.

Fig. 3a–c shows photographs of the PBS- and AuNP-spotted membranes. It can be seen that the AuNP spots could hardly be discerned in the images, especially for the membrane with the lower AuNP concentration. The same membranes were imaged using the PT-LSI sensor. Time-lapse speckle images acquired over a period of 10 seconds for each case are presented in Supplementary Movie. For a better visualization of the PT-induced speckle modulations, the central regions of the AuNP spots (1 mm x 0.8 mm in size) are shown in the movie. It can be noted that the speckle pattern from the membrane with a high concentration of AuNPs produced a significantly large modulation, while the membranes with a lower AuNP concentration and PBS exhibited smaller modulations. In the resultant PT-LSI images (Fig. 3d–f), the AuNP spots can be clearly visualized. Interestingly, a small PT-LSI signal was observed in the PBS-only case. This result suggests the occurrence of an intrinsic PT response from the nitrocellulose membrane. Such PT response of nitrocellulose membranes has indeed been

reported in a previous publication (Qin et al. 2012). The PT excitation of the nitrocellulose membrane may cause the thermal deformation of the membrane, which would subsequently lead to a speckle modulation. It should be noted, though, that PT-LSI signals from the AuNPs are significantly greater than those from AuNP-free regions. Hence, our PT-LSI sensor can differentiate and visualize the distribution of AuNPs against AuNP-free regions in the membrane.

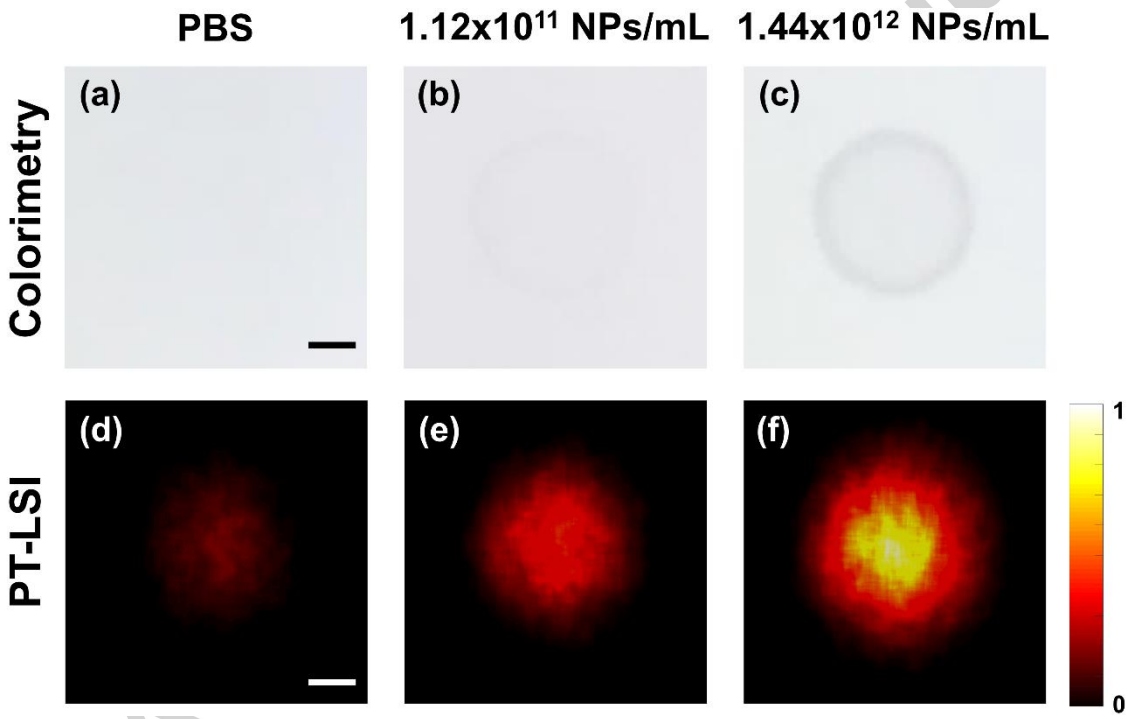

Fig. 3. PBS- and AuNP-spotted nitrocellulose membranes imaged using colorimetric (a–c) and PT-LSI sensors (d–f). Small concentrations of AuNPs could hardly be visualized in the colorimetric image, but could be discerned in the PT-LSI images. The scale bar denotes 1 mm.

We then examined the dependence of PT-LSI output on the PT light intensity. For these measurements, three nitrocellulose membranes were prepared, and two of which were

pipetted with 1 μL of PBS and 1 μL of AuNP solution (1.44×10^{12} NPs/mL), respectively. The membranes were then measured with the PT-LSI sensor for different PT light intensities. To obtain the PT-LSI output for each membrane, the ROIs were defined as circles with a radius of 2.5 mm and their centers at the highest PT-LSI values. We then evaluated the mean of the PT-LSI pixel values over the ROI. Fig. 4 shows the PT-LSI outputs as a function of PT light intensity for the membranes with no specimen, PBS-only, and AuNPs. It can be noted that the PT-LSI output from the AuNP-spotted membrane increases linearly with PT light intensity. However, the PT-LSI outputs from the AuNP-free membranes (i.e., bare and PBS-spotted membranes) also exhibited linear behaviors, although the slopes are smaller. As described earlier, it can be explained by the intrinsic PT response of the membrane. The use of higher PT light intensities may thus provide PT-LSI outputs with higher magnitudes, but the noise-equivalent PT-LSI outputs from the AuNP-free membranes also increase linearly. Therefore, the ratio of the PT-LSI outputs of the AuNP-spotted to AuNP-free membranes does not depend on PT light intensity in our case.

Our PT-LSI results for the bare nitrocellulose membranes indicate that the measurement error due to the fluctuation of the cellulose nitrate concentration in the membrane is not large. Specifically, the standard error of the PT-LSI outputs for the bare membrane were measured to be 3.70 for the PT light intensity of 1.5 mW/mm^2, while for the same operating condition, the mean PT-LSI output was 472.95. Hence, the uncertainty of our PT-LSI measurements arising from the variation of the cellulose nitrate concentration in the employed membranes (HF13502XSS, Millipore, USA) is estimated to be <1% of the mean PT-LSI output.

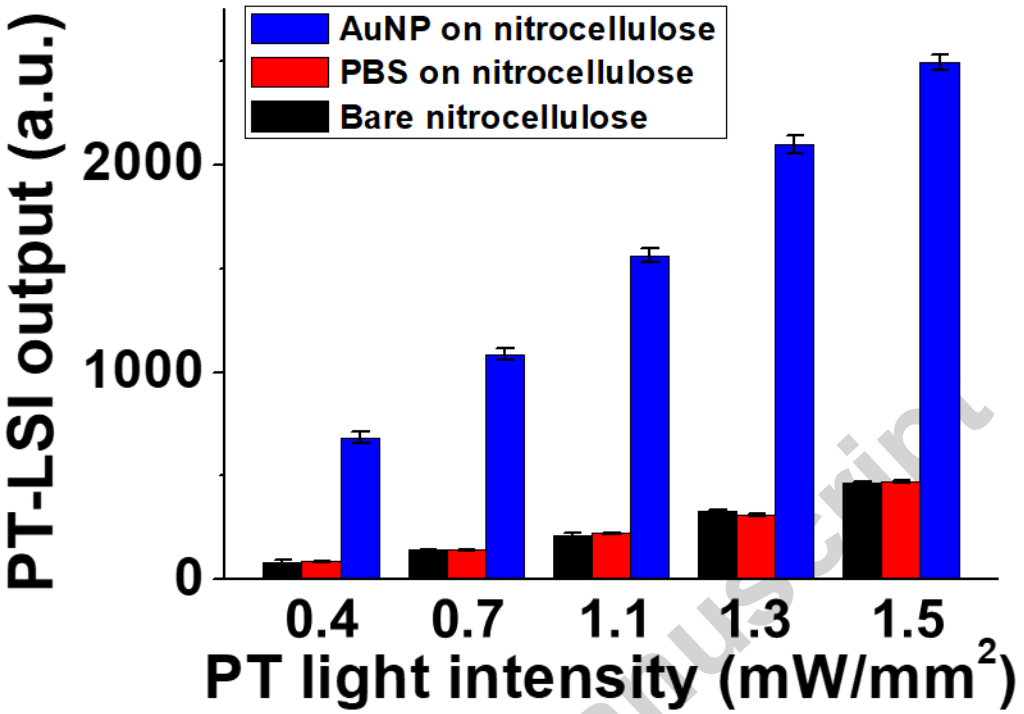

Fig. 4. PT-LSI outputs of the bare nitrocellulose membrane and membranes spotted with PBS and AuNPs (1.44×10^{12} NPs/mL), measured at various PT light intensities. PT-LSI output from the AuNPs-spotted membrane increased linearly with the PT light intensity. PT-LSI outputs from the nitrocellulose membranes with no specimen and PBS-only also exhibited linear behaviors, but with smaller slopes. Error bars represent standard error (n=3).

3.2. Detection limit comparison of PT-LSI and colorimetric sensors

In order to demonstrate the superior analytical performance of the PT-LSI versus the colorimetric sensors, AuNP solutions of varying concentrations ranging from 1.14×10^{9} to 1.44×10^{12} NPs/mL were prepared (see Section 2.4). Each AuNP solution was then pipetted onto nitrocellulose membranes, and the membranes were dried for 10 minutes prior to colorimetric

and PT-LSI imaging. Measurements for the membrane with PBS only were also performed and used as the noise-equivalent output for each analysis.

Shown in Fig. 5a are photographs of the AuNP-spotted membranes. It is evident that as the AuNP concentration is smaller, the AuNP spot on the membrane becomes invisible. We chose the region of measurement to be a circle with a radius of 2.5 mm centered at the field of view, and then the colorimetric and PT-LSI outputs were evaluated (Fig. 5b). A detailed description on the colorimetric analysis is provided in Supplementary Information. The solid lines denote the fits performed with four-parameter logistic function (Supplementary Information, Table S1). We estimated the detection limit of each sensor as the concentration corresponding to noise-equivalent output (i.e., control) plus 3 times standard deviation of its replicates. The detection limits of the colorimetric and PT-LSI sensors were measured to be 4.08×10^{11} NPs/mL and 3.29×10^{9} NPs/mL, respectively, indicating that the detection limit of the PT-LSI sensor was 125 times smaller than that of the colorimetric sensor.

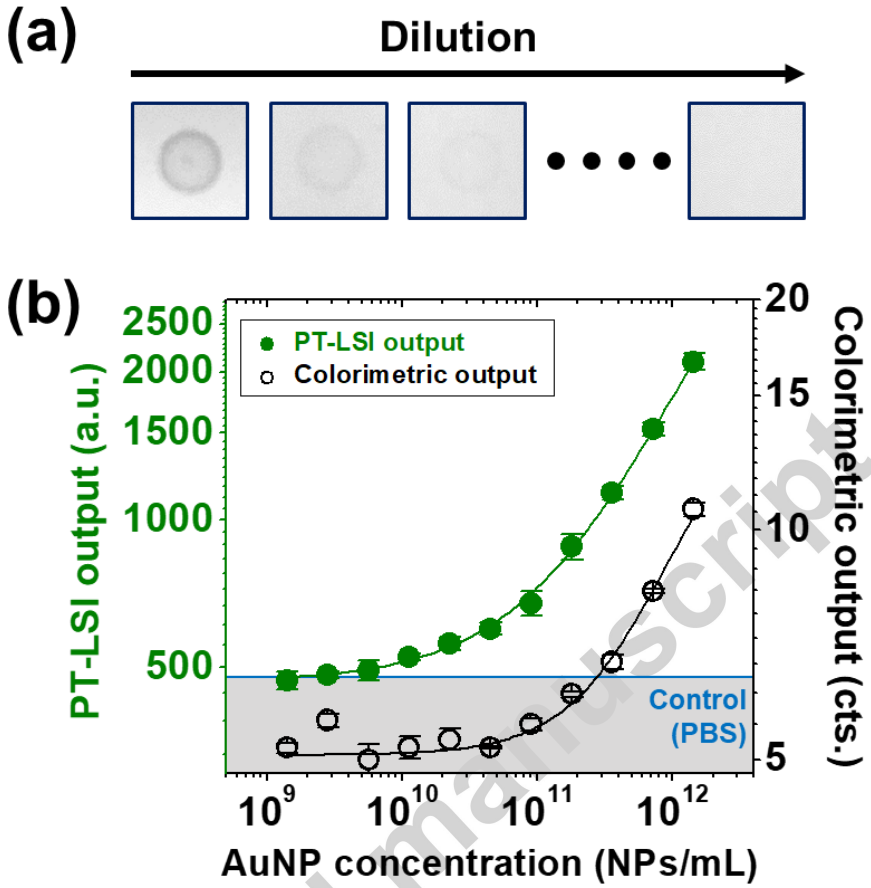

Fig. 5. PT-LSI vs. colorimetric sensors for AuNP-spotted membranes. (a) Photographs of AuNP-spotted membranes with various AuNP concentrations. (b) Dose response curves of PT-LSI and colorimetric sensors for the AuNP-spotted nitrocellulose membrane. Error bars represent standard error (n=5).

3.3. PT-LSI assay of CrAg meningitis LFA

HIV-related cryptococcal meningitis continues to cause a substantial amount of deaths in low- and middle-income countries (Park et al. 2009; Vidal and Boulware 2015). The diagnosis of CrAg in serum and cerebrospinalsecsss fluid by latex agglutination tests or enzyme-linked immunoassays has been available for many years, but the associated detection methods often

require trained operators and sophisticated laboratory equipment. Recently, paper-based LFA kits capable of providing semi-quantitative CrAg measurements have been approved by the U.S FDA, and have been used for the diagnosis of cryptococcosis with little or no laboratory infrastructure.

We performed PT-LSI imaging of the CrAg LFA kits to assess its utility as a highly sensitive LFA detector for clinically-relevant disease biomarkers. CrAg-positive solutions were prepared by serial two-fold dilution of CrAg-positive stock solution (CrAg concentration ~ 500 ng/mL, REF CB1020, IMMY Inc., USA). The solutions were then loaded into the cartridges and dried for 10 minutes prior to colorimetric and PT-LSI imaging.

Fig. 6a shows photographs of the CrAg LFA cartridges after the reactions were complete. We performed the colorimetric and PT-LSI imaging both in the control and test lines in an LFA chip, and the measurements with the control line responses larger than three times the noise-equivalent outputs were considered valid. Note that the colorimetric and PT-LSI measurements of the PBS-only chips were used as the noise-equivalent outputs. The LFA chips that reacted with solutions of lower CrAg concentrations exhibited a smaller visual contrast in the test line, which is a characteristic of sandwich-type LFAs. The dose response curves of the colorimetric and PT-LSI sensors are shown in Fig. 6b. The dose curves were fitted using four-parameter logistic functions (Table S1). The detection limits of the colorimetric and PT-LSI sensors were measured to be 1:140 titer and 1:9480 CrAg titer, which approximately corresponds to 3.57 ng/ml and 0.052 ng/ml, respectively. This result suggests that the detection limit of the PT-LSI sensor was 68 times superior to that of the colorimetric sensor in this particular LFA chips.

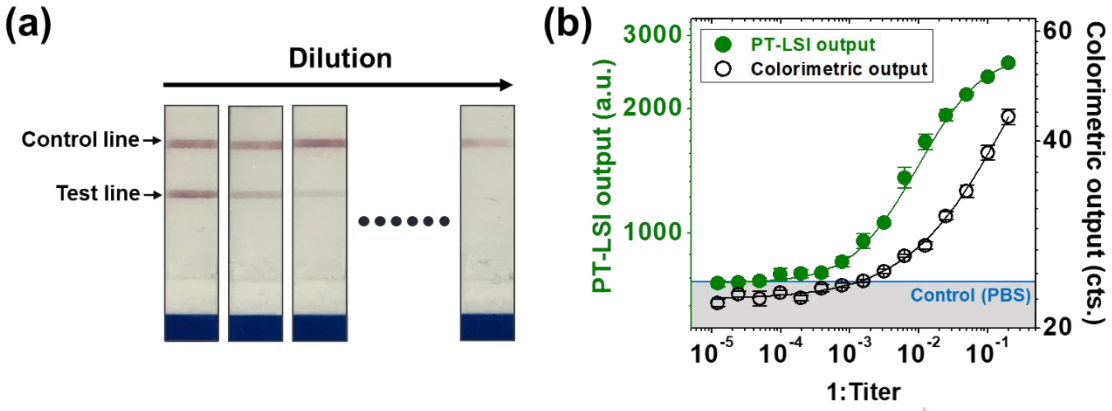

Fig. 6. PT-LSI vs. colorimetric sensors for the CrAg LFA cartridges. (a) Photographs of the CrAg LFA membranes after reacting with specimens of various CrAg concentrations. (b) Dose response curves of the PT-LSI and colorimetric sensors. The PT-LSI sensor featured a detection limit 68 times smaller than that of the colorimetric sensor. The blue line denotes the noise-equivalent output, which was acquired with LFA cartridges containing PBS only. Error bars represent standard error (n=5).

Serum-based CrAg screening and preemptive antifungal therapy in patients with advanced AIDS help to stop the clinical progression to symptomatic meningitis. Non-invasive CrAg assay with urine specimens would greatly help with diagnosis and subsequent treatment, but the concentration of CrAg in urine is 22 times lower than in blood (Jarvis et al. 2011). Therefore, the presented sensitivity of the PT-LSI sensor holds a great promise for non-invasive screening of asymptotic people with AIDS and for the quantification of the CrAg to stratify the future risk of developing the symptomatic disease.

One may note that the enhancement factors of the detection limit of the PT-LSI sensor in the AuNPs and CrAg assays against those of the colorimetric sensor were different (125x versus 68x compared with the colorimetric sensor). This may be accounted for by the differences in

physical size, surface treatment, and the functionalization of the AuNPs and substrate membranes in each assay. These differences may result in different LSPR resonance signatures of the AuNPs. Measurements of the LSPR properties in CrAg LFA chips and subsequent PT-LSI optimization would further enhance the PT-LSI sensitivity for the CrAg assay.

4. Discussion

One of the notable features of our sensor is that it enables simple, inexpensive, and highly sensitive detection in conventional LFA cartridges. Because it does not involve any modification of the detection cartridge, commercial LFA chips can be directly measured by the PT-LSI sensor. Furthermore, the sensor can be readily miniaturized to a small footprint using inexpensive consumer-grade optoelectronic devices. More specifically, in our demonstration, the PT-LSI sensor was implemented by employing an optical chopper for modulating the PT excitation light and a CMOS camera for high-speed image acquisition. However, PT light modulation can be implemented by direct current modulation of the laser diodes or using a microcontroller, such as Arduino. The high-speed CMOS camera can also be replaced by inexpensive webcams, which cost less than $20. PT-LSI implementation with such inexpensive and miniaturized components would result in a portable and inexpensive, yet highly sensitive LFA sensor.

The detection limit of our sensor is largely determined by the intrinsic PT response of the nitrocellulose membrane. As noted by the previous publication (Qin et al. 2012) and our results (Fig. 3 and 4), the membrane itself exhibited speckle modulation under PT light illumination, which acts as the background in our measurements. Other materials such as polyether sulfone (Edwards and Baeumner 2006; Kalogianni et al. 2007) and polyethylene (Fernández-Sánchez et

al. 2005) have been explored for replacing nitrocellulose for LFA membranes. The PT responses of these materials have not been investigated, but the use of a material with a smaller PT response could further improve the PT-LSI detection limit. Other metallic nanoparticles with higher PT responses could also be employed for improving sensitivity. Metallic nanoparticles with other geometries (e.g., nanoshells and nanorods) have been found to exhibit strong LSPR response, which can be several orders-of-magnitude higher than that of AuNPs (Qin et al. 2012). Assay development with these nanoparticles and PT-LSI optimization for such assays would enable high-sensitivity screening of many biomarkers that could not be detected via colorimetric sensors.

In our computational platform (Intel Xeon CPU @ 2.10GHz CPU and 32GB memory), the PT-LSI output was obtained in ~2.5 min. However, this computational speed can be enhanced with various hardware/software-based strategies. For instances, instead of computing Fourier transform of the intensity fluctuation on each pixel, inner product of the intensity fluctuation with the Fourier basis function of the PT modulation frequency can be evaluated to obtain the PT-LSI signal at each pixel. This approach does not require Fourier transform and could potentially facilitate computational speed. We are also investigating pulsed or coded PT light illumination and the associated signal processing (Donoho 2006; Eldar and Kutyniok 2012), which could make the computation faster. The integration of these methods with high-speed field programmable gate array (FPGA) devices would make our sensor a rapid and viable LFA detector.

Our present demonstration was performed with an FDA-approved CrAg assay. Our future studies will involve PT-LSI assays of diverse biomarkers with patient-derived specimens.

Exemplary applications include the measurement of C-reactive proteins (CRPs) or various biomarkers for infectious diseases in human salivary specimens. CRPs, for example, are present in extremely small amounts in saliva (approximately 10 ng/mL) (Ouellet-Morin et al. 2011), and their detection has thus been performed mainly with fluorescence-based detectors. The demonstrated high sensitivity of the PT-LSI sensor would enable the detection of such small amounts of biomarkers with no additional chemistry and LFA chip modification. Recent progress in LFA technologies has also enabled the multiplexing of various biomarkers in a single LFA chip. As PT-LSI is an imaging setup, it enables simultaneous detection of various biomarkers on a single LFA chip without modification of the imaging hardware. Certainly, diverse strategies for antibody-antigen binding to deal with a wide range of biochemical substances should also be explored.

5. Conclusion

We presented a simple and inexpensive optical sensor for highly sensitive LFA assay. The sensor exploited the high sensitivity of PT-LSI to perform the quantification of biomarkers absorbed in LFA membranes. Our sensor measured AuNPs in the range of 1.14×10^{9} to 1.44×10^{12} NPs/mL with a detection limit of 3.26×10^{9} NPs/mL, which corresponds to a 125-fold enhancement in detection limit compared with colormetric sensor. The PT-LSI sensor was then utilized to perform CrAg assay, demonstrating the detection with a sensitivity 68 times higher compared with the colorimetric sensor.

Our sensor requires no modifications of the conventional LFA chip designed for colorimetric assay. Therefore, it can be immediately employed to measure commercial LFA chips. The PT-LSI

sensor also features portability, simplicity and low cost of implementation and operation. The sensor can be readily built with inexpensive laser pointers and webcams, and can thus be miniaturized to a small form factor. We believe these features make PT-LSI a promising LFA sensing platform in point-of-care settings.

ACKNOWLEDGMENT

The authors would like to thank the staff at Mirimedix Inc. for providing the nitrocellulose membranes and AuNPs. This work was supported by the research program of the National Research Foundation of Korea (NRF) (No. 2015R1A5A1037668).

REFERENCES

Ahn, J.S., Choi, S., Jang, S.H., Chang, H.J., Kim, J.H., Nahm, K.B., Oh, S.W., Choi, E.Y., 2003. Development of a point-of-care assay system for high-sensitivity C-reactive protein in whole blood. Clinica chimica acta 332(1-2), 51-59.

Briers, J.D., Webster, S., 1996. Laser speckle contrast analysis (LASCA): a nonscanning, full-field technique for monitoring capillary blood flow. Journal of biomedical optics 1(2), 174-180.

Donoho, D.L., 2006. Compressed sensing. IEEE Transactions on information theory 52(4), 1289-1306.

Edwards, K.A., Baeumner, A.J., 2006. Optimization of DNA-tagged dye-encapsulating liposomes for lateral-flow assays based on sandwich hybridization. Analytical and bioanalytical chemistry 386(5), 1335-1343.

Eldar, Y.C., Kutyniok, G., 2012. Compressed sensing: theory and applications. Cambridge University Press.

Fernández-Sánchez, C., McNeil, C.J., Rawson, K., Nilsson, O., Leung, H.Y., Gnanapragasam, V., 2005. One-step immunostrip test for the simultaneous detection of free and total prostate specific antigen in serum. Journal of immunological methods 307(1-2), 1-12.

Huang, Y., Ng, S., Liu, L., Li, C., Chen, Y., Hung, Y., 2009. NDT&E using shearography with impulsive thermal stressing and clustering phase extraction. Optics and Lasers in Engineering 47(7-8), 774-781.

Hung, Y., Chen, Y.S., Ng, S., Liu, L., Huang, Y., Luk, B., Ip, R., Wu, C., Chung, P., 2009. Review and comparison of shearography and active thermography for nondestructive evaluation. Materials Science and Engineering: R: Reports 64(5-6), 73-112.

Jarvis, J.N., Percival, A., Bauman, S., Pelfrey, J., Meintjes, G., Williams, G.N., Longley, N., Harrison, T.S., Kozel, T.R., 2011. Evaluation of a novel point-of-care cryptococcal antigen test on serum, plasma, and urine from patients with HIV-associated cryptococcal meningitis. Clinical infectious diseases 53(10), 1019-1023.

Kalogianni, D.P., Goura, S., Aletras, A.J., Christopoulos, T.K., Chanos, M.G., Christofidou, M., Skoutelis, A., Ioannou, P.C., Panagiotopoulos, E., 2007. Dry reagent dipstick test combined with 23S rRNA PCR for molecular diagnosis of bacterial infection in arthroplasty. Analytical biochemistry 361(2), 169-175.

Khreich, N., Lamourette, P., Boutal, H., Devilliers, K., Créminon, C., Volland, H., 2008. Detection of Staphylococcus enterotoxin B using fluorescent immunoliposomes as label for immunochromatographic testing. Analytical biochemistry 377(2), 182-188.

Kim, G., Lim, J., Mo, C., 2015. A Review on Lateral Flow Test Strip for Food Safety. Journal of Biosystems Engineering 40(3), 277-283.

Leuvering, J.H., Thal, P., Waart, M.v.d., Schuurs, A., 1980. Sol particle immunoassay (SPIA). Journal of immunoassay 1(1), 77-91.

Lin, Y.-Y., Wang, J., Liu, G., Wu, H., Wai, C.M., Lin, Y., 2008. A nanoparticle label/immunochromatographic electrochemical biosensor for rapid and sensitive detection of prostate-specific antigen. Biosensors and Bioelectronics 23(11), 1659-1665.

Liu, J., Mazumdar, D., Lu, Y., 2006. A Simple and Sensitive "Dipstick" Test in Serum Based on Lateral Flow Separation of Aptamer-Linked Nanostructures. Angewandte Chemie 118(47), 8123-8127.

Maiolini, E., Ferri, E., Pitasi, A.L., Montoya, A., Di Giovanni, M., Errani, E., Girotti, S., 2014. Bisphenol A determination in baby bottles by chemiluminescence enzyme-linked immunosorbent assay, lateral flow immunoassay and liquid chromatography tandem mass spectrometry. Analyst 139(1), 318-324.

Martinez, A., Phillips, S., Whitesides, G., Carrilho, E., 2010. Diagnostics for the developing world: microfluidic paper-based analytical devices. Analytical chemistry 82(1), 3.

Mauriz, E., Calle, A., Manclus, J., Montoya, A., Lechuga, L., 2007. Multi-analyte SPR immunoassays for environmental biosensing of pesticides. Analytical and bioanalytical chemistry 387(4), 1449-1458.

Mirasoli, M., Buragina, A., Dolci, L.S., Guardigli, M., Simoni, P., Montoya, A., Maiolini, E., Girotti, S., Roda, A., 2012. Development of a chemiluminescence-based quantitative lateral flow immunoassay for on-field detection of 2, 4, 6-trinitrotoluene. Analytica chimica acta 721, 167-172.

Ngom, B., Guo, Y., Wang, X., Bi, D., 2010. Development and application of lateral flow test strip technology for detection of infectious agents and chemical contaminants: a review. Analytical and bioanalytical chemistry 397(3), 1113-1135.

Ouellet-Morin, I., Danese, A., Williams, B., Arseneault, L., 2011. Validation of a high-sensitivity assay for C-reactive protein in human saliva. Brain, Behavior, and Immunity 25(4), 640-646.

Park, B.J., Wannemuehler, K.A., Marston, B.J., Govender, N., Pappas, P.G., Chiller, T.M., 2009. Estimation of the current global burden of cryptococcal meningitis among persons living with HIV/AIDS. Aids 23(4), 525-530.

Posthuma-Trumpie, G.A., Korf, J., van Amerongen, A., 2009. Lateral flow (immuno) assay: its strengths, weaknesses, opportunities and threats. A literature survey. Analytical and bioanalytical chemistry 393(2), 569-582.

Qin, Z., Chan, W.C., Boulware, D.R., Akkin, T., Butler, E.K., Bischof, J.C., 2012. Significantly improved analytical sensitivity of lateral flow immunoassays by using thermal contrast. Angewandte Chemie International Edition 51(18), 4358-4361.

Quesada-González, D., Merkoçi, A., 2015. Nanoparticle-based lateral flow biosensors. Biosensors and Bioelectronics 73, 47-63.

Stolyarov, A.M., Sullenberger, R.M., Crompton, D.R., Jeys, T.H., Saar, B.G., Herzog, W.D., 2015. Photothermal speckle modulation for noncontact materials characterization. Optics letters 40(24), 5786-5789.

Tripathi, P., Upadhyay, N., Nara, S., 2017. Recent advancements in lateral flow immunoassays: A journey for toxin detection in food. Critical reviews in food science and nutrition, 1-20.

Vidal, J.E., Boulware, D.R., 2015. Lateral flow assay for cryptococcal antigen: an important advance to improve the continuum of hiv care and reduce cryptococcal meningitis-related mortality. Revista do Instituto de Medicina Tropical de São Paulo 57, 38-45.

Whang, D.H., Um, T., 2005. Comparison of immunochromatography assays and quantitative immunoassays for detecting HBsAg and anti-HBs. The Korean Journal of Laboratory Medicine 25(3), 186-191.

Xia, X., Xu, Y., Zhao, X., Li, Q., 2009. Lateral flow immunoassay using europium chelate-loaded silica nanoparticles as labels. Clinical chemistry 55(1), 179-182.
Zhao, Y., Huang, Y., Zhao, X., McClelland, J.F., Lu, M., 2016. Nanoparticle-based photoacoustic analysis for highly sensitive lateral flow assays. Nanoscale 8(46), 19204-19210.
Zhu, J., Chen, W., Lu, Y., Cheng, G., 2008. Development of an immunochromatographic assay for the rapid detection of bromoxynil in water. Environmental pollution 156(1), 136-142.

Supplementary Movie: Time-lapse laser speckle images of PBS- and AuNP-spotted membranes under the 2-Hz modulated PT light illumination. In order to better visualize the PT-induced speckle modulations, the central regions of the membranes are presented. The speckle pattern from the membrane with a high concentration of AuNPs ($2.0x10^{12}$ NPs/ml) produced a markedly large modulation, while the membranes with a lower AuNP concentration ($1.0x10^{11}$ NPs/ml) and PBS exhibited smaller modulations.

Highlights

- A novel optical sensor for paper-based immunoassay is described.
- Exploits high-sensitivity of laser speckle to photothermal optical and mechanical perturbations of LFA membrane.
- Demonstrates 68-125x improved detection limit compared to colorimetric sensor.
- Simple to operate and implement.